The Dynamics of the $O(^1D) + HCl \rightarrow OH + Cl$ Reaction at a 0.26 eV Collision Energy: A Comparison between Theory and Experiment†

P. Bargueño,‡ P. G. Jambrina,§ and J. M. Alvariño

Departamento de Química Física, Universidad de Salamanca, 37008 Salamanca, Spain

M. L. Hernández

Departamento de Física de la Atmósfera, Universidad de Salamanca, 37008 Salamanca, Spain

F. J. Aoiz, M. Menéndez, and E. Verdasco

Departamento de Química Física, Facultad de Química, Universidad Complutense, 28040 Madrid, Spain

T. González-Lezana*

Instituto de Física Fundamental (CSIC), Serrano 123, 28006 Madrid, Spain

Received: March 16, 2009; Revised Manuscript Received: April 24, 2009

The dynamics of the $O(^1D) + HCl(v = 0, j = 0) \rightarrow Cl + OH$ reaction at a 0.26 eV collision energy has been investigated by means of a quasiclassical trajectory (QCT) and statistical quantum and quasiclassical methods. State-resolved cross sections and Cl atom velocity distributions have been calculated on two different potential energy surfaces (PESs): the H2 surface (Martínez et al. *Phys. Chem. Chem. Phys.* **2000**, *2*, 589) and the latest surface by Peterson, Bowman, and co-workers (PSB2) (*J. Chem. Phys.* **2000**, *113*, 6186). The comparison with recent experimental results reveals that the PSB2 PES manages to describe correctly differential cross sections and the velocity distributions of the departing Cl atom. The calculations on the H2 PES seem to overestimate the OH scattering in the forward direction and the fraction of Cl at high recoil velocities. Although the comparison of the corresponding angular distributions is not bad, significant deviations with a statistical description are found, thus ruling out a complex-forming mechanism as the dominant reaction pathway. However, for the ClO + H product channel, the QCT and statistical predictions are found to be in good agreement.

I. Introduction

In addition to the nonreactive deactivation into $O(^3P)$,[1] the collision between an $O(^1D)$ atom and HCl can proceed via the two possible reaction pathways

$$O(^1D) + HCl \rightarrow OH + Cl \quad (1)$$

$$O(^1D) + HCl \rightarrow ClO + H \quad (2)$$

Both reactions have been extensively studied in the past. A number of experiments under thermal conditions have enabled the measurement of product distributions of the OH fragments formed in reaction 1.[2−5] The measured vibrational distributions are inverted, with a ratio of about 1.5 between the population observed for the $OH(v' = 1)$ product fragments and those in the vibrational ground state $OH(v' = 0)$[2] and maximum peaks at $v' = 3$ and 4.[3,4] Alexander et al.[6] studied the $O(^1D) + HCl \rightarrow OH(v' = 4, N = 6) + Cl$ reaction at an average collision energy $E_c \approx 0.55$ eV using the technique of polarized photoinitiated reaction in conjunction with Doppler-resolved, polarized LIF detection. The analysis of their results yielded the product state-resolved differential cross section (DCS) and relative excitation function for that particular rovibrational state. Products were found to be predominantly scattered in the backward ($\theta \approx 180°$) and to a lesser extent in the forward ($\theta \approx 0°$) directions with basically no sideways scattering ($\theta \approx 90°$). In turn, Casavecchia and co-workers,[7] using crossed molecular beams (CMBs) with mass spectrometry detection, measured the ClO product angular distribution and time-of-flight (TOF) spectra at several laboratory (LAB) scattering angles for reaction 2 at a 0.529 eV (12.2 kcal mol^{-1}) collision energy. The resulting center-of-mass (CM) angular distribution, fairly forward−backward symmetric, was analyzed in terms of a superposition of a backward component and a symmetric backward−forward component that would correspond to two distinct mechanisms: a direct abstraction of the halogen atom on the ground singlet potential energy surface (PES) of OHCl and that arising from the formation of a long-lived complex as a consequence of an insertion mechanism via the HOCl intermediate.

Only recently, a series of experiments have been performed to obtain global angle-resolved information on reaction 1. Suzuki and co-workers[8,9] have used CMBs and imaging detection of the Cl coproduct via (2 + 1) REMPI of the $^2P_{3/2,1/2}$ states. Triple angle−velocity distributions in the CM frame were extracted

† Part of the "Vincenzo Aquilanti Festschrift".

* To whom correspondence should be addressed. E-mail: tglezana@imaff.cfmac.csic.es.

‡ Also Instituto de Física Fundamental (CSIC), Serrano 123, 28006 Madrid, Spain.

§ Also Departamento de Química Física, Facultad de Química, Universidad Complutense, 28040 Madrid, Spain.

10.1021/jp902336s
Published on Web 05/28/2009

from the images at several collision energies by determining the angular and velocity distributions of the $Cl(^2P_{3/2})$ atoms. The angular distributions present certain asymmetry between the peaks at the forward and at the backward scattering directions, which was found to vary with the collision energy from $E_c = 0.1821$ eV (4.2 kcal mol^{-1}) to $E_c = 0.2775$ eV (6.4 kcal mol^{-1}). At the lowest collision energy, the observed DCS exhibits a nearly forward−backward symmetry, whereas at the highest E_c (0.2775 eV) the distribution presents a slight preference for the forward scattering direction.[9] However, the most salient feature of the extracted angle−velocity polar maps was the absence of CM recoil velocities of the Cl atoms associated with vibrationally/rotationally cold OH products. Although the resolution of the experiments and the congestion of OH internal states due to the high exoergicity did not allow the identification of individual rovibrational peaks, it became evident that states $v' = 0$, 1 and rotational states $j' = 0-15$, associated with the largest Cl velocities, were practically absent.

In recent years, several PESs have been calculated for the $1^1A'$ ground singlet state of this system. Hernández et al.[10] produced a global PES based on CASSCF and MRCI electronic structure calculations, and a functional based on expansion in bond order coordinates was used for the fit. The PES was subsequently refined[11] (hereafter H2 PES) and proved to be accurate to reproduce the experiments of the group of Perugia[7] for reaction 2 using quasiclassical trajectory (QCT) calculations. Bowman, Peterson, and co-workers have produced a PES (PSB1) for this system[12−14] which was later improved[15,16] (hereafter designated as PSB2). Finally, Nanbu et al.[17] have performed extensive calculations to determine not only the ground $1^1A'$ PES but also the two lowest excited states, $1^1A''$ and $2^1A'$. The $1^1A''$ state correlates with both product channels, but its transition state for reaction 2 is too high to be accessed at low collision energies. The $2^1A'$ state only correlates with the OH + Cl products via a relatively high (0.28 eV) transition state.

Common to all these ab initio calculations is the fact that the ground $1^1A'$ PES for the title reaction exhibits two wells ∼4.4 and ∼1.94−2.05 eV deep (measured from the asymptotic energy of the $O(^1D)$ + HCl reactants) which correspond, respectively, to the equilibrium geometries for the HOCl and HClO isomers. This circumstance together with the high exoergicity (1.92 eV for reaction 1) and the heavy−light−heavy kinematics of the system makes exact quantum methods (EQMs) extremely demanding in terms of computational time,[18] requiring partial waves up to $J = 120$ and a large basis of rovibrational channels. These numerical difficulties explain why most of the existing theoretical work consists on QCT calculations.[9−11,16,19−24] Quantum mechanical (QM) calculations have been restricted to a zero total angular momentum, $J = 0$, with different helicity decoupling approximations invoked when the $J > 0$ case was considered.[15,18,25−32]

One of the issues investigated in some detail deals with the possible participation of excited electronic states on the overall dynamics of the $O(^1D)$ + HCl collision. The excited $1^1A''$ and $2^1A'$ PESs seem to play a significant role according to the analysis performed at $J = 0$ of the product branching ratio and vibrational distributions for OH.[27] The study of reaction probabilities,[28,29] vibrational distributions,[29] and product internal energy distributions[9] reveals different dynamics in the excited electronic states in comparison with the ground PES. Recent experimental and theoretical investigations of the DCSs concluded, however, that reaction 1 proceeds predominantly via the ground electronic state at collision energies of less than 0.2819 eV (6.5 kcal mol^{-1}).[9]

In this work we have restricted our analysis to the ground surface using two of the above-mentioned PESs for the title reaction available in the literature: the PES by Peterson, Bowman, and co-workers (PSB2)[15] and the surface by Hernández and co-workers (H2).[11] Although both PESs have strong resemblances and their overall dynamics are qualitatively similar, a more careful inspection reveals significant differences. For the OH + Cl product channel, noticeable discrepancies are found in the vibrational distributions obtained on both surfaces, whereas for the vibrational cross sections calculated at $E_c = 0.53$ eV by Christoffel et al.[16] with the PSB2 PES peak at $OH(v' = 3)$, in agreement with some of the experimental results at thermal energies,[3,4] the corresponding distributions obtained with the H2 surface manifest a preference for the $v' = 2$ state.[11] For the ClO + H channel, equivalent translational energy distributions have been found with both PESs.[11,22] However, the H2 PES predicts a substantially higher product branching ratio for the ClO formation.

In spite of the above-mentioned inverted vibrational distributions observed for reaction 1, the insertion of the $O(^1D)$ atom into the H−Cl bond, forming a short-lived highly excited HOCl complex, which fragments before the energy is randomized, was invoked as the main dynamical mechanism in some of the pioneering studies.[2,4,5,19] Theoretical work following the experiments of ref 7 confirmed that the overall dynamics of the $O(^1D)$ + HCl collision was strongly determined by the double-well topology of the PES, resulting in more than just a unique reaction mechanism.[10,11,20,23,24] Thus, trajectories exploring the deeper HOCl well were associated with the above-mentioned insertion mechanism,[23] responsible for the backward peaks in both the DCS for formation of ClO in reaction 2[11,23] and the angular distribution for reaction 1.[11] In turn, trajectories that visit the less deep HClO well, with shorter lifetimes than those in the HOCl well, describe the attachment of the O atom onto the HCl side. These trajectories coming from the HClO species were found to originate the inverted vibrational population of the $OH(v')$ fragments[11,23] and the forward peaks in the DCSs for both reactions 1 and 2.[11] This scenario has been described even in more detail by Martínez et al.,[24] who identified both qualitatively and quantitatively the different dynamical features observed in a large variety of magnitudes such as opacity functions, DCSs, vibrational cross sections, and recoil velocity distributions originated by trajectories exploring the HOCl well, the HClO well, or both wells consecutively. The authors of ref 24 concluded that although the O + HCl → OH + Cl reaction mainly involves at least the deep HOCl potential well (if not both wells), for sufficiently short collision times, the underlying mechanism cannot be simply described as an insertion process mediated by the formation of a long-lived intermediate complex; even trajectories oscillating between both wells were found to give rise to a vibrational inversion.

Despite this seemingly important contribution from "non-trapped" collisions to the overall dynamics of the $O(^1D)$ + HCl reaction, the existence of the deep double-well potential structure has motivated the use of statistical approaches in the past to study the title process. An early example is found in the study by Luntz[2] in which measurements of the rotational distributions for the OH fragment were compared with statistical predictions obtained with phase-space theory (PST) and a rigid rotor harmonic oscillator treatment. The deviations of the calculated distributions with respect to the experimental values were interpreted as an indication of a fast fragmentation of the HOCl

complex before a complete equipartition of the energy. A similar conclusion was inferred in the REMPI study of Matsumi et al.[5] performed at an average collision energy of about 0.33 eV from the differences observed between the measured average product translational energy for the OH + Cl channel and the values calculated from a prior distribution estimate. In the same work, the detected isotope effect on the reaction branching ratio [OCl + H]/[OH + Cl], equal to 0.24, smaller when the H atom is substituted by a D atom, was not reproduced by PST and prior distributions. Although the vibrational distribution for the product OH fragments cannot be reproduced statistically,[4] the analysis of the corresponding rotational distributions by means of statistical approaches has led some authors to suggest some sort of complex-forming mechanism for the O + HCl → OH + Cl reaction. Thus, rotational distributions obtained by means of a statistical Monte Carlo algorithm were found to be in fairly good agreement with the experimental values reported in ref 2, especially for the OH($v' = 0$, $j' \leq 20$) rotational states. More recently, a simple statistical calculation (possibly performed by counting the energetically accessible rovibrational states of the corresponding diatom fragments) of the cumulative reaction probability for $J = 0$ showed that the EQM results largely deviate from those of the simple statistical analysis.[27] In a qualitative manner, an osculating complex model was employed by Kohguchi et al.[9] to explain the observed preference in the DCSs for the forward scattering direction as the collision energy increases. With this model, a simple estimate of the collision time (τ_{coll}) can be obtained assuming that the intermediate complex corresponds to the equilibrium geometry of the HOCl well. τ_{coll} was found to increase as E_c decreases. In particular, at $E_c = 0.2775$ eV, $\tau_{coll} \approx 340$ fs, somewhat larger than that calculated with QCT on the H2 PES at 0.53 eV (~190 fs).[24] The most recent QCT calculations for reaction 1 on the PES of Nanbu et al.,[17] also reported in ref 9, could not account for the details of the measured angular distributions obtained in the experimental studies of Suzuki and co-workers.[8,9] Thus, the ratio between the forward and backward scattering directions found at $E_c = 0.26$ eV in the measurements of ref 8 seems to differ from the corresponding value obtained in the QCT calculation.[9] In addition, the apparent dependence of the shape of the DCS on the energy observed in the experiment was not evident in the results from the trajectory studies.

In an attempt to provide some further insight into the overall dynamics of the O(^{1}D) + HCl → OH + Cl reaction, we have undertaken the study of this reaction at $E_c = 0.26$ eV, which corresponds to the experiments of ref 8, using the QCT method and the statistical quantum[33,34] and quasiclassical[35−37] methods (SQM and SQCT, respectively). The purpose is 2-fold. On one side, we try to investigate how far a rigorous SQM approach can describe the dynamics of this reaction channel. On the other side, we intend to assess the quality of the above-mentioned PESs by contrasting the newest experimental results on reaction 1 with those obtained by using the H2 and PSB2 PESs. The former PES proved to be very accurate to describe the experimental results for reaction 2, but it has not been tested against global, angle−velocity-resolved experimental data for reaction 1.

This paper is structured as follows: In section II the specific details of the SQM and QCT methods are provided. In section III we present the results, which are further discussed in section IV. Finally, the conclusions are presented in section V.

II. Theory

A. Quasiclassical Trajectory Calculation. The general QCT methodology here employed has been extensively described in previous works, and only some brief details will be given here.

Batches of 2×10^6 and 5×10^5 trajectories have been calculated on the $1^1A'$ H2[11] and PSB2[15] PESs, respectively, for the title reaction and initial HCl rovibrational state ($v = 0$, $j = 0$) at $E_c = 0.260$ eV (6 kcal mol^{-1}) that corresponds to the average collision energy of the CMB experiments of Kohguchi and Suzuki (KS).[8] An integration step of 0.025 fs ensured a conservation of total energy and total angular momentum better than 1 in 10^5 and 10^7, respectively. Trajectories were started and finished at a distance from the atom to the CM of the diatom of 10 Å to ensure no interaction between them. The maximum impact parameter was set at 3.35 Å.

The usual histogramatic method to assign the final product's states consists in rounding the classical (real value) vibrational and rotational quantum numbers to their nearest integers. Given the relatively large vibrational actions of the OH molecule, this rounding procedure may cause severe distortions of the classical rovibrational distributions, allowing the population of states that are energetically close. As in previous works,[38] we have used here the Gaussian binning method[39,40] whose implementation has been described in detail.[38] Briefly, it consists in weighting each trajectory according to Gaussian functions centered on the right QM vibrational action, in such a way that the closer the vibrational (real value) quantum number of a given trajectory to the nearest integer, the larger the weighting coefficient for that trajectory will be. In the present work we have used a full width at half-maximum for the Gaussian functions of 0.15. Changing this value from 0.1 to 0.25 does not significantly affect the results. For the ClO + H channel, since the rovibrational states are closely spaced, the usual binning method does not lead to significant errors. The results for this product channel were practically identical to those obtained with the Gaussian binning approach.

The reactive DCSs, $d^2\sigma_R/d\omega$, were calculated by the method of moments expansion in Legendre polynomials.[41,42] The Smirnov−Kolmogorov test comparing the cumulative probability distributions was used to decide where the series can be truncated. The error bars, calculated as in ref 41, correspond to ±1 standard deviation. Similarly, the CM Cl product velocity (w_{CL}) distributions were calculated by the method of moments expansion in Legendre polynomials using the reduced variable $r = 2(w_{CL}/w_{max}) - 1$, where w_{max} is the maximum Cl recoil velocity allowed by the energy conservation. Finally, the QCT triple angle−velocity DCS (angle−velocity polar maps) were determined by fitting the results to a double series of Legendre polynomials with arguments cos θ and r.[42] In all cases, the coefficients of the single and double distributions were calculated by weighting the trajectories with their Gaussian binning weights.

B. Statistical Quantum and Classical Methods. The SQM has been extensively described on a number of occasions before. The interested reader is referred to refs 33 and 34 for a further description of the technical details. In essence, the method was originally designed to describe the overall dynamics of reactions proceeding via the formation of a collision complex. Individual capture probabilities, $p^{IJ}_{vj\Omega}(E)$, for the complex to be formed from a specific rovibrational $vj\Omega$ state of the reactant fragments at specific values of the total angular momentum (J) and the QM parity (I) are calculated by solving the corresponding coupled-channel equations with a log derivative method from a chosen capture radius, R_{cap}, up to the asymptotic region, represented,

TABLE 1: Comparison between the Capture Probabilities for Different (v', j', $\Omega' = 0$) Rovibrational States of the OH Product Fragment Calculated, at Several Values of the Total Angular Momentum J, with the SQM Approach Employing the Subsets [0, 10] and [0, 16][a]

	($v' = 0$, $j' = 3$)		($v' = 1$, $j' = 10$)		($v' = 2$, $j' = 0$)		($v' = 3$, $j' = 10$)	
J	[0, 10]	[0, 16]	[0, 10]	[0, 16]	[0, 10]	[0, 16]	[0, 10]	[0, 16]
0	0.97405	0.99679	0.95612	0.99272	0.97414	0.98775	0.96766	0.96924
5	0.99449	0.99923	0.95613	0.99278	0.97449	0.98794	0.96820	0.96932
10	0.99357	0.99910	0.95936	0.99276	0.97584	0.98796	0.96955	0.97003
15	0.99362	0.99910	0.95962	0.99290	0.97672	0.98796	0.97029	0.97049
20	0.99344	0.99908	0.95921	0.99299	0.97736	0.98607	0.97066	0.96977
25	0.99364	0.99909	0.95746	0.99208	0.97558	0.98430	0.97007	0.96829

[a] See the text for details.

in practice, by a certain R_{max} value. The v, j, and Ω QM numbers refer to the vibrational state, the diatom rotational state, and the value of the component of **J** along the z axis of the body-fixed reference frame, respectively. For the product channel, the analogous capture probabilities, hereafter referred to as $p^{J}_{v'j'\Omega'}(E)$, divided by the total sum over all the possible arrangement channels and rovibrational states, can be interpreted as the probabilities for the complex to fragmentate via those specific states. The state-to-state reaction probability is then approximated as the product of the capture probabilities for the initial and final states divided by the sum of the corresponding probabilities for all energetically open states in both reactant and product arrangements. DCSs can be calculated after a random phase approximation which neglects the contribution from the interference terms coming from different J partial waves is invoked.[34] The method has been successfully applied to investigate the dynamics of different insertion reactions.[43,44]

The SQM calculation has been performed here in its Coriolis coupling version with no helicity decoupling approximations. For the product arrangements, however, the huge number of existing OH(v', j') and, especially, ClO(v'', j'') rovibrational states complicates enormously the computational evaluation of the corresponding capture probabilities. To overcome this difficulty, we have followed a procedure similar to the method employed in ref 45, where the calculations were carried out by using a sequence of independent runs with a limited number of rotational states j between 0 and the actual j_{max} value with a non-negligible capture probability for each product channel. The convergence of this approach is tested by comparison with results obtained with different sizes of the [j_a, j_b] subsets considered in each run. For illustration purposes, we present in Table 1 the comparison, for different values of the total angular momentum, of the capture probabilities for the O(^{1}D) + HCl $\rightarrow$ Cl + OH reaction obtained in SQM calculations in which the rotational basis set for the OH fragment is restricted to [$j = 0$, $j = 10$] and [$j = 0$, $j = 16$]. The values of the probabilities for different OH(v', j', Ω') rovibrational states corresponding to the calculation with the smaller rotational basis, much less numerically demanding, are however in sufficiently good agreement with the values obtained with the larger basis set to ensure the convergence. A similar comparison, for the product H + ClO arrangement, is shown in Table 2 at $J = 10$ for different ($v'' = 0$, j'', $\Omega'' = 0$) rovibrational states of the ClO product diatom between calculations with a [$j'' = 0$, $j'' = 30$] basis set and those obtained with the larger [$j'' = 0$, $j'' = 60$] basis. Apart from the difference observed for the probability of the upper limit of the lower subset, the $j'' = 30$ state, the agreement found between both sets of results certainly encourages the use of the smaller basis. The discrepancy of the specific cases at the boundaries of the subsets defined to reduce the computational difficulty does not affect however the calculation of average quantities and can be, on the other hand, easily corrected when a state-to-state description is required.

TABLE 2: Same as in Table 2, but with Comparison between the Capture Probabilities at $J = 10$ for the ClO($v'' = 0$, j'') + H Product Channel for the SQM Calculations Performed with a Restricted Set of ClO Rotational Levels between [0, 60] and [0, 30]

	[0, 60]	[0, 30]
($j'' = 10$, $\Omega'' = 0$)	0.75670	0.74898
($j'' = 15$, $\Omega'' = 0$)	0.63444	0.62360
($j'' = 20$, $\Omega'' = 0$)	0.59845	0.58865
($j'' = 29$, $\Omega'' = 0$)	0.50260	0.48954
($j'' = 30$, $\Omega'' = 0$)	0.48562	0.27304

TABLE 3: Parameters of the SQM Calculations for the Three Possible Arrangements O + HCl, Cl + OH, and H + ClO[a]

	R_{cap}	R_{max}	j_{max}	[0, j_1], [$j_1 + 1$, j_2],..., [j_i, j_{max}]
O + HCl	2.5	5.8	20	[0, 20]
Cl + OH	2.3	3.4	32	[0,10],[11,21],[22,32]
H + ClO	2.4	9.7	86	[0,30],[31,61],[62,86]

[a] In the second and third columns, values for the capture radius, R_{cap}, and for R_{max}, the value for the asymptotic region, are measured in angstroms. In the fifth column the sequence of different diatom rotational state windows used in the calculation is shown (see the text for details).

Values for the rotational states involved in each calculation, for the capture radii, R_{cap}, for the maximum distance used to describe the asymptotic region, R_{max}, and for the largest rotational state, j_{max}, are given in Table 3. As shown in the table, the calculation for the two product channels has been separated into three different rotational subsets. For the H + ClO case, some especially high partial waves required an additional reduction of the size of such divisions.

The QCT version of the statistical model has also been extensively described in previous works.[35−37] In all respects, the assumptions and methodology are identical to those of the SQM model except for the fact that trajectories instead of wave functions are propagated in the entrance and exit channels. This model also accounts for the conservation of parity, and it is inherently a type of calculation without any decoupling. Its only possible limitation with respect to the SQM model is the neglect of tunneling, since zero-point energy effects and microscopic reversibility are correctly accounted for by the model. Usually, this method is much less computationally demanding, especially when, as in the present case, the number of product channels is very large. The results obtained with the SQCT model on the H2 PES are almost identical with those obtained with the SQM model, and they will not be discussed in this paper. The SQCT results on the PSB2 PES will be shown in some instances to

demonstrate that the statistical results are similar on both PESs in spite of the important differences found in the respective QCT calculations.

To determine the (normalized) Cl atom recoil velocity distribution integrated over scattering angles from the (v', j') state resolved integral cross section (ICS), $\sigma(v', j')$, we have used the following equation:

$$P(w_{Cl}) = \sum_{v'j'} \frac{\sigma(v',j')}{\sigma_R} N \exp\left[-\frac{(w_{Cl} - w_{v'j'})^2}{\Delta w^2}\right] \quad (3)$$

where w_{Cl} is given in terms of the relative translational energy of the products, E'_{trans}, by

$$w_{Cl} = \left[\frac{2m_{OH}}{m_{Cl}M} E'_{trans}\right]^{1/2} \quad (4)$$

In eq 3, σ_R is the total reactive cross section for OH formation, N is the normalization constant, and $w_{v'j'}$ is the Cl atom CM recoil velocity associated with the (v', j') rovibrational state of OH, whose value is given by

$$w_{v'j'} = \left[\frac{2m_{OH}}{m_{Cl}M}(E_{tot} - E_{v'j'})\right]^{1/2} \quad (5)$$

where M is the total mass and the total energy available to the products, E_{tot}, is given by the energy balance:

$$E_{tot} = E_c + \Delta D_0 + E_{v,j} = E'_{trans} + E_{v'j'} \quad (6)$$

E_c is the collision energy, $\Delta D_0 = -\Delta H_0^0$ is the difference in the dissociation energies of the products and reactants from their zero-point energies (reaction exoergicity), and $E_{v,j}$ and $E_{v'j'}$ are the reagent's (HCl) and product's (OH) internal energies, respectively, calculated from their zero-point values. In the present case the initial state of HCl is $v = j = 0$ and $E_{v,j} = 0$.

The Gaussian function that appears in eq 3 with a width Δw is used to simulate the experimental resolution, which has been taken to be constant in the whole range of recoil velocities.

Similarly, the CM triple angle−velocity DCS can be calculated from the state-to-state DCS, $d\sigma_R/(d\omega\, dw_{Cl})$, as

$$P(\theta, w_{Cl}) = \frac{1}{\sigma_R}\frac{d\sigma_R}{d\omega\, dw_{Cl}} = \frac{1}{\sigma_R}\sum_{v'j'}\left(\frac{d\sigma_R}{d\omega}\right)_{v'j'} N \exp\left[-\frac{(w_{Cl} - w_{v'j'})^2}{\Delta w^2}\right] \quad (7)$$

If the DCS is calculated for a restricted range of recoil velocities, it is sufficient to integrate over the chosen range of w_{Cl}; i.e.

$$P(\theta, w_1', w_2') = \int_{w_1'}^{w_2'} P(\theta, w_{Cl})\, dw_{Cl} \quad (8)$$

Finally, the distribution of recoil velocities for a restricted range of scattering angles [θ_0, θ_1] can be written as

$$P(w_{Cl}, \theta_0, \theta_1) = 2\pi \int_{\theta_0}^{\theta_1} P(\theta, w_{Cl}) \sin\theta\, d\theta \quad (9)$$

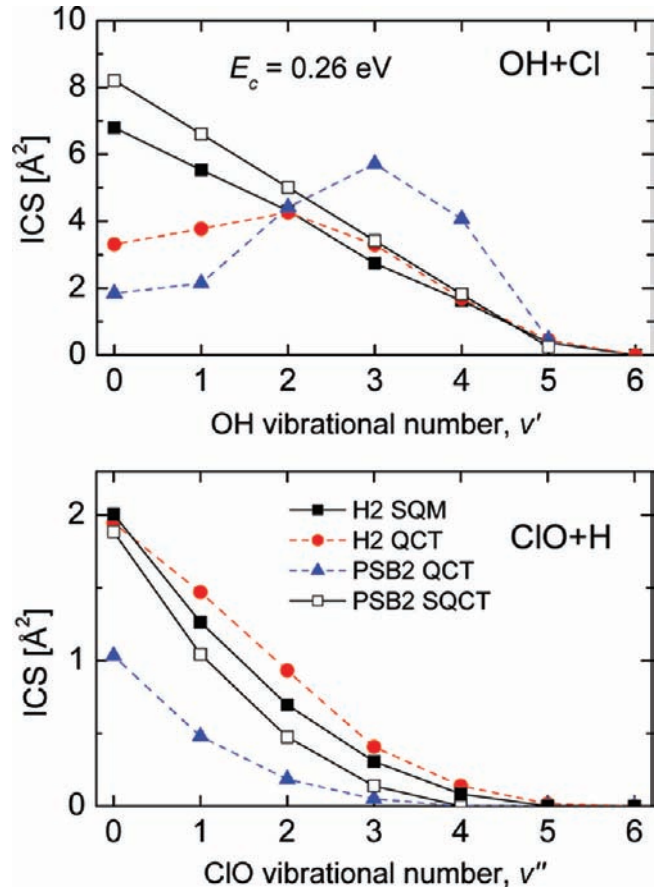

Figure 1. Vibrationally resolved ICSs for the O + HCl($v = 0, j = 0$) → OH(v') + Cl (top panel) and O + HCl($v = 0, j = 0$) → ClO(v'') + Cl (bottom panel) reactions (Å^2) at $E_c = 0.26$ eV. SQM and QCT results for the H2 PES are shown as full squares and full circles, respectively, while the QCT and SQCT distributions for the PSB2 PES are respectively shown as full triangles and open squares.

III. Results

In this section we show the results of our investigation on the dynamics of the title reaction at $E_c = 0.26$ eV with the SQM, SQCT, and QCT approaches presented above. Theoretical predictions at this particular collision energy will be compared with the recent experimental work by KS.[8] Given the above-mentioned subtle differences on some dynamical features found in previous investigations, we have employed both the H2 PES by Martínez et al.[11] and the PSB2 potential[15,16] for the ground $1^1A'$ electronic state.

A. Rovibrational Cross Sections. The vibrationally resolved ICSs for the O(^{1}D) + HCl($v = 0, j = 0$) reaction at the 0.26 eV collision energy on both surfaces are shown in Figure 1 for the OH- and ClO-forming product channels. One of the most interesting features found for the case of the OH + Cl arrangement is the distinct shape exhibited by the QCT vibrational distributions depending on which surface is employed. In both cases the vibrational cross sections display an inverted structure wherein the production of the OH fragment in $v' > 0$ is the preferred outcome of the collision. However, the prediction for the maximum peak varies from $v' = 2$ to $v' = 3$ for the H2 and PSB2 PESs, respectively. As for the ClO + H channel, although the shapes of the vibrational distributions are similar and there is no vibrational inversion in either case, the difference in their absolute values is remarkable, in agreement with previous results.[11,16]

The statistical predictions for reaction 1, also shown in Figure 1, do not deviate enormously from the QCT distributions on

TABLE 4: ICSs (Å^2) at $E_c = 0.26$ eV Calculated with the QCT, SQM, and SQCT Approaches on the H2 and PSB2 PESs for Both Cl + OH and H + ClO Product Channels

	H2 QCT	H2 SQM	H2 SQCT	PSB2 QCT	PSB2 SQCT
Cl + OH	16.8	21.4	20.94	18.6	25.3
H + ClO	4.9	4.3	4.2	1.7	3.5

the H2 PES. As expected, the OH vibrational inversion cannot be reproduced by the SQM (or SQCT) approach, and only the decay as v' increases of the populations for those OH vibrational states $v' > 2$ is in some accordance with the QCT results on the H2 surface. The agreement between the QCT and statistical results obtained with the PSB2 PES is even poorer. One may argue that these discrepancies could be due to differences between the two PESs. However, the SQCT calculations on the PSB2 PES, also shown in the figure, yield very similar results for the two PESs.

The agreement between the QCT and SQM vibrationally resolved cross sections on the H2 PES is significantly better for the ClO-forming channel as it has no vibrational inversion. Although the ClO(v'') QCT distribution obtained on the PSB2 PES also decreases monotonically with v'', its value is about half that obtained on the H2 surface for most of the vibrational states for this reaction channel. Interestingly, the predictions of the SQCT model on the PSB2 PES are much closer to the results on the H2 PES than to the full dynamical QCT calculations on the PSB2 PES.

Similar comparisons can be extended to the total cross sections. Values of the ICSs summed over all final vibrational states for each product channel at a 0.26 eV collision energy are shown in Table 4. Despite the differences observed in the OH vibrational distribution, the values of the total ICSs are not extremely sensitive to the PES employed in the QCT calculation: The value of 16.8 Å^2 obtained with the H2 PES is somewhat smaller than but not too far from the result on the PSB2 PES (18.6 Å^2). The SQM at this collision energy predicts a higher total cross section σ_R than that predicted by the QCT calculations. This seems to be the result of the excess in the population observed for OH($v' = 0$ and 1) in the statistical distribution in comparison with the QCT result.

The SQM and QCT total cross sections for the ClO + H channel on the H2 PES are close to each other, as shown in Table 4. However, the deviation from the value obtained using QCT on the PSB2 PES is remarkable, and the cross sections on the two PESs differ by almost a factor of 3. Calculations using the SQCT method on the PSB2 PES predict a relatively minor deviation from those obtained on the H2 PES with similar cross section values, far from those obtained with QCT. This fact confirms that the main difference between both PESs is connected to the topology of the wells, which are not explored by either of the two statistical approaches.

The QCT results on the PSB2 PES shown in Table 4 are in good accord with previous trajectory and QM results on the same PES.[15,16] The cross sections summed over both reaction channels are very similar on both PESs and also close to the value obtained by Lin et al. on an earlier surface[18] (~22 Å^2). In summary, the PSB2 PES predicts a somewhat higher contribution of the OH + Cl channel at the expense of the ClO + H channel, whose reactivity is significantly diminished. It is also apparent that, with regard to the total and vibrationally resolved cross sections, the statistical approach is fairly accurate for the ClO reaction channel; it deviates to some extent in the case of the OH + Cl channel on the H2 PES and fails completely to account for the branching ratio in the case of the PSB2 PES.

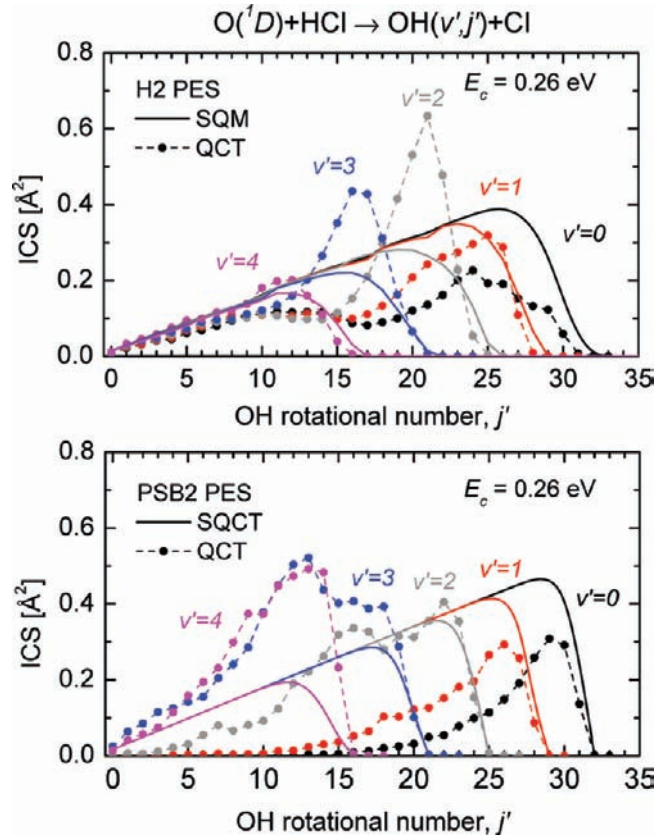

Figure 2. Rotational cross sections for O + HCl($v = 0$, $j = 0$) → OH(v', j') + Cl at a 0.26 eV collision energy: (top panel) distributions obtained on the H2 surface and (bottom panel) distributions obtained on the PSB2 PES by means of the QCT approach (dashed line and full circles) and of the SQM approach (solid line). Cross sections for the OH($v' = 0$) final state are shown in black, OH($v' = 1$) in red, OH($v' = 2$) in gray, OH($v' = 3$) in blue, and OH($v' = 4$) in magenta.

The rotational distributions for the OH vibrational states from $v' = 0$ to $v' = 4$ are shown in Figure 2. The distributions are rotationally hot, exhibiting the largest values for relatively high j' states in each vibrational manifold. This trend is however slightly different for the $v' = 2$ and 3 levels on the PSB2 PES, whose distributions seem to present a bimodal character. The peak on the corresponding vibrational distributions (see Figure 1) at $v' = 2$ for the H2 surface has its origin in a well-developed maximum around $j' \approx 21$. The explanation for the $v' = 3$ peak on the PSB2 PES is the largely populated $j' = 10-14$ rotational states (which also constitute the maximum for the $v' = 4$ manifold).

The main noticeable difference between the QCT rotational distributions on both PESs is the absence of population of the lowest rotational states for $v' = 0$ and $v' = 1$ on the PSB2 PES. While the tail of the corresponding distributions on the H2 PES extends to the lowest rotational levels for these vibrational levels, there seems to be a cutoff at $j' \approx 15$ in the case of the PSB2 PES. Low j' states only appear in the $v' = 3$ and 4 manifolds, showing, in addition, higher cross sections than on the H2 surface. This implies that OH will appear only in states with a considerable internal excitation.

The rotational distributions predicted by the SQM and SQCT models conform to the expected behavior for statistical treatments wherein the populations increase gradually with j' up to a maximum and then decay rapidly on the basis of the conservation of the energy and angular momentum. Although the detailed dynamical behavior cannot be accounted for by the

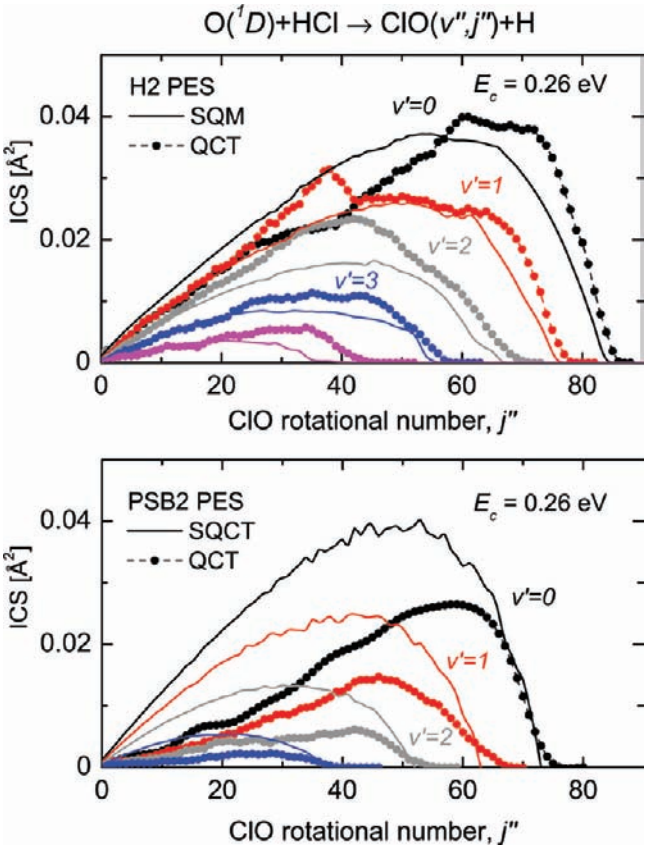

Figure 3. Same as Figure 2 for the O + HCl($v = 0, j = 0$) → ClO (v'', j'') + H channel.

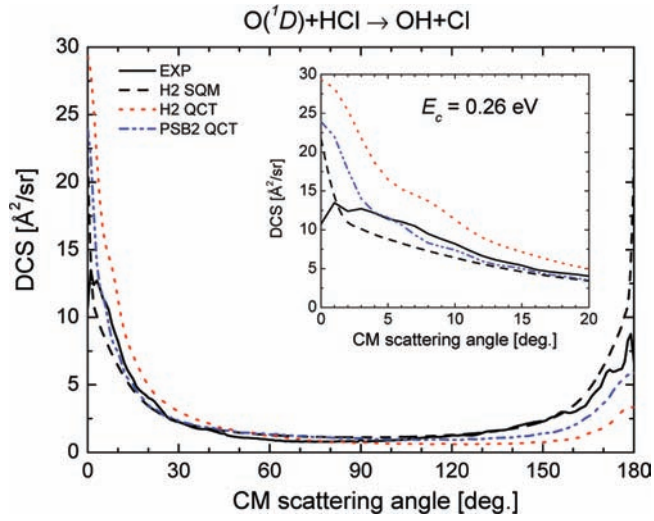

Figure 4. Comparison between the experimental DCS of ref 8 (black solid line) and present theoretical DCSs (Å^2 sr^{-1}) for O + HCl($v = 0$, $j = 0$) → OH + Cl at $E_c = 0.26$ eV. SQM cross sections calculated on the H2 PES are shown as a black dashed line, QCT results on the H2 PES are shown as a red dotted line, and QCT results on the PSB2 PES are shown as a blue dashed−dotted line. The experimental distribution has been scaled to match the theoretical predictions at the $\theta = 90°$ scattering direction. The inset corresponds to a magnified view of the $0° \leq \theta \leq 20°$ angular region close to the forward scattering direction.

SQM on the H2 PES, the statistical results are found to describe correctly the energy distribution among the different j' states for the largest OH($v' = 4$) and OH($v' = 5$) levels, the latter not shown here.

The SQCT model applied to the PSB2 PES renders rotational distributions that, apart from somewhat higher cross section values, agree very well with the corresponding results on the H2 PES. The deviation from the QCT results is indeed more striking for this PES.

For completeness purposes, the rotational distributions for the H + ClO product channel are shown in Figure 3. The shapes of the QCT dynamical and statistical treatments are in better overall accord than for the OH formation channel, although the maxima for the various v'' manifolds are shifted to higher rotational states in the QCT calculations. The most apparent difference, as commented on above, is the smaller cross sections obtained on the PSB2 PES for most rovibrational levels. Comparing the statistical results on both PESs, the accordance is fairly decent. Clearly, the QCT results on the PSB2 PES deviate most from the statistical behavior.

B. Differential Cross Sections. One of the observables investigated in ref 8 is the DCS for the title reaction. In Figure 4 the experimental DCS transformed to the CM frame is compared with the corresponding statistical prediction and the QCT results using the two surfaces considered here. The measured distribution has been scaled to match the theoretical DCSs at the $\theta = 90°$ scattering direction.

The QCT distributions exhibit a sharp peak at the forward direction, which is clearly at odds with the implicit forward−backward symmetry of any statistical prediction. Moreover, the SQM prediction on the H2 PES for $\theta = 0°$ (see the inset of Figure 4), 21.7 Å^2 sr^{-1}, is lower than the corresponding QCT value on the same PES, 29.3 Å^2 sr^{-1}, but turns out to be close to the DCS on the PSB2 PES, 23.9 Å^2 sr^{-1}. The large ratio between the DCS values in the forward and backward directions of the QCT distributions (∼8.8 on the H2 PES and ∼4.1 on the PSB2 surface) causes the statistical DCS to overestimate the QCT cross sections at the backward direction. The overall comparison with the experiment reveals that the outcome of the QCT calculations on the PSB2 PES leads to a somewhat better theoretical accordance, the only significant deviation being at the forward scattering direction. In the recent trajectory study reported in ref 9, the DCS calculated at the same collision energy, $E_c = 0.26$ eV, on the PES by Nanbu et al.[17] exhibits peaks of ∼10 and ∼3 Å^2 sr^{-1} at the forward and backward directions, respectively, yielding therefore an only slightly smaller value for the above-mentioned forward/backward ratio than the present results on the PSB2 PES. In the experimental distribution[8] the ratio between forward and backward peaks is about 1.6, significantly below the findings obtained with any of the above-mentioned QCT calculations. Nevertheless, this comparison has to be taken with care since the resolution in the experiment for the extreme forward and backward angles is biased by the solid angle size at those scattering angles.

The slight asymmetry observed in the measured cross section was interpreted by the authors of ref 8 as indicative of an osculating complex whose lifetime would be shorter than the average rotational time associated with a hypothetical intermediate complex. The present comparison between the SQM and the experimental angular distribution reveals, however, sufficiently good agreement to ascribe some importance to the complex-forming mechanism during the course of the reaction. The only noticeable deviation with respect to the measured DCS is found in the precise value at the backward peak where the calculated cross section is considerably larger.

The investigation of the DCS performed in the experimental study of KS includes an analysis for different velocity regimes for the product Cl fragment, w_{Cl}. The DCS extracted for low

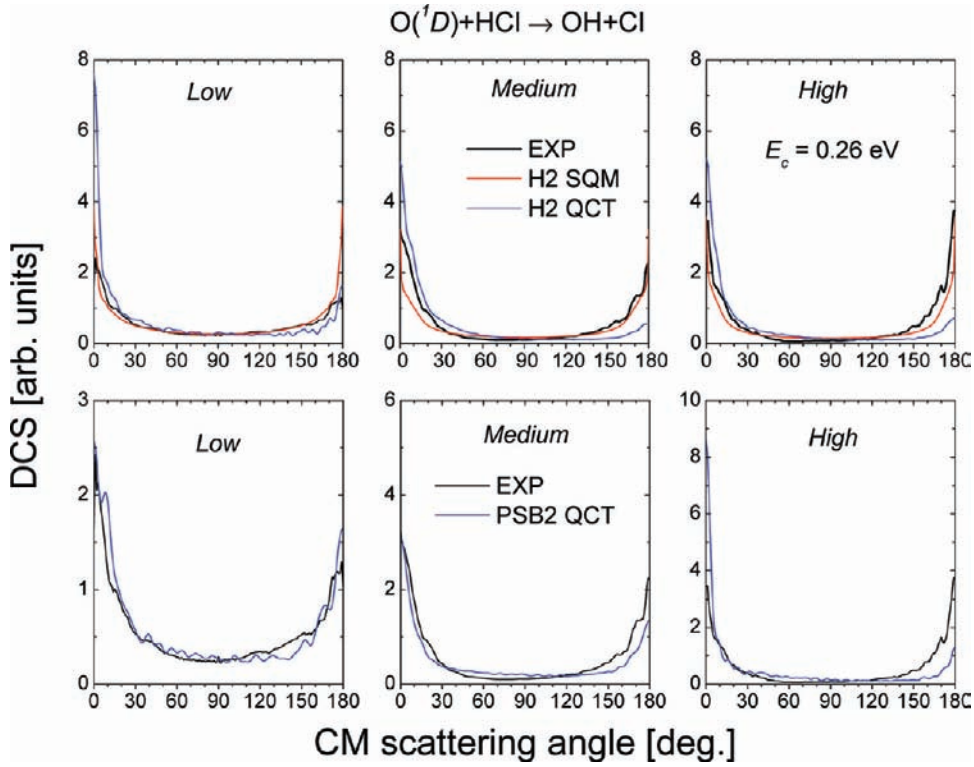

Figure 5. DCSs for the low (left panels), medium (middle panels), and high (right panels) Cl velocity ranges as defined in ref 8. The experimental angular distributions (black line)[8] are compared for each velocity regime with SQM (red line) and QCT (blue line) obtained with the H2 PES (top panels) and with the PSB2 surface (bottom panels). See the text for details.

(0−580 m s^{-1}), medium (580−1170 m s^{-1}), and high (1170−1750 m s^{-1}) ranges of the Cl recoil velocity revealed an interesting angular behavior: a gradual variation from a forward peaked distribution to an overall symmetrical profile with respect to the sideways direction as w_{Cl} increases. In this work, we have also calculated DCSs for the above-described Cl velocity intervals by means of the SQM and QCT methods using eq 8. Note that the upper limit established in ref 8 for the high velocity regime, 1750 m s^{-1}, effectively excludes some OH rovibrational states, specifically the ($v' = 0, j' = 0-14$) and ($v' = 1, j' = 0-4$) states, which correspond to $w_{Cl} > 1750$ m s^{-1}.

The comparison of theoretical DCSs calculated on both PESs with the experimental results[8] is shown in Figure 5 for the three different Cl velocity regimes. In this case, the partial DCSs displayed in each panel have been scaled to the experimental data by using the same partial ICSs (integrating the DCS multiplied by sin θ over the whole range of scattering angles). The top panel of Figure 5 includes the comparison between the QCT and SQM results on the H2 PES together with the experimental results of Kohguchi et al.[8]

The angular distribution measured for the high Cl velocity regime exhibits a symmetric profile around the sideways direction. For the other two regimes, corresponding to chlorine atom velocities which do not exceed 1170 m s^{-1}, certain asymmetry, as in the case of the total DCS, is observed. The QCT result shows a prominent peak at the $\theta \approx 0°$ direction for the three velocity regimes. While the agreement of the trajectory results on the H2 PES with the experimental DCSs is certainly poor, the statistical predictions manage to describe the measured angular distributions, the only deviation being some overestimation of the forward and backward peaks for the low velocity regime.

The comparison of the measured distributions and those obtained with the trajectory calculation on the PSB2 PES reveals good agreement in the low and medium velocity ranges, which is in contrast with that found on the H2 surface.

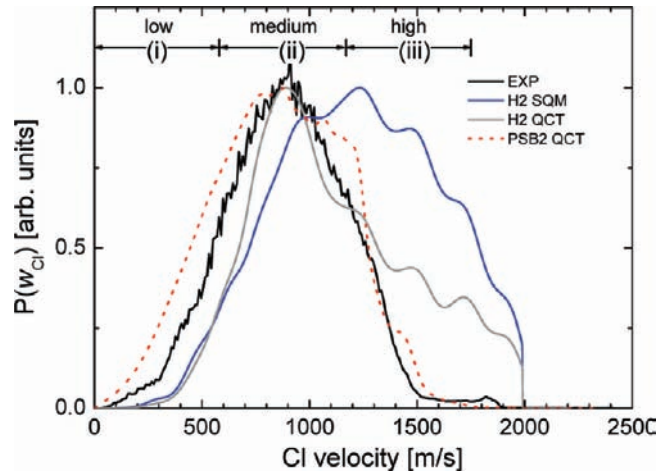

Figure 6. Comparison between the experimental Cl velocity distribution, adapted from ref 8 (black solid line), and the present statistical results (blue solid line) obtained with the H2 surface and QCT distributions calculated on the H2 surface (gray solid line) and on the PSB2 PES (red dotted line). Cl velocity regimes have been defined at the top.

C. Velocity Distributions. The experimental detection of the recoil velocities of the Cl atoms, w_{Cl}, enabled the authors of ref 8 to obtain probability density functions in terms of such a quantity. In this work, we have employed the present QCT and SQM approaches to obtain the corresponding theoretical counterparts. The probability functions $P(w_{Cl})$ have been calculated with eq 3 considering the contribution from all energetically accessible OH rovibrational states. The comparison of theoretical and experimental results is shown in Figure 6.

The measured distribution presents a clear predominance of velocities from the medium range, with smaller contributions

from velocities above 1170 m s^{-1} or below 580 m s^{-1}. The QCT $P(w_{Cl})$ values on both surfaces peak at approximately the same w_{Cl} as the experimental distribution, but the agreement of the results on the PSB2 PES with the experimental data is clearly better. The corresponding velocity distribution for the H2 surface shows a contribution from the fastest Cl atoms which seems to be absent in the measured result. The differences from both QCT distributions can be easily explained by inspection of the respective rotational distributions (see Figure 2) and can be traced back to the populations of those internal states of OH with the lowest content of internal energy. In particular, the populations found for the OH($v' = 0, j' \leq 25$) and OH($v' = 1, j' \leq 21$) states, which produce Cl atoms with $w_{Cl} > 1170$ m s^{-1}, have non-negligible ICSs in the calculations on the H2 PES, while in the case of the PSB2 PES, the OH($v' = 0, 1, j' < 15$) states are not populated at all by the reaction, and the highest possible Cl velocities are absent.

There are significant deviations of the statistical results (the SQCT on the PSB2 PES, not shown) from the experimental distribution. The maximum of the SQM function appears to be shifted to a larger velocity than the peak exhibited by both the experimental result and the QCT distributions. In addition, the overestimation of the probability of finding the Cl atom at its largest possible velocity is noticeable.

The analysis of the experimental study in ref 8 included OH internal energy probability distributions in terms of the CM scattering angle. In this work, we have carried out a similar analysis in terms of w_{Cl}, decomposing the total velocity distribution of Figure 6 in their contributions from forward, sideways, and backward scattering angles, using eq 9. The OH internal energy results of Figure 7 of ref 8 have been transformed to produce the corresponding Cl recoil velocity distributions. The comparison of such experimental results and those calculated by means of the present QCT and SQM theoretical approaches is portrayed in Figure 7 for the three CM scattering angle intervals.

The maximum of the experimental $P(w_{Cl}, \Delta\theta)$ distributions moves slightly from 900 m s^{-1} at forward angles to ~1100 m s^{-1} in the backward direction. The overall profile is found to change slightly, with the development of a secondary maximum in the case of the forward region or the extension to larger velocities for both the forward and backward regions. The description provided by the QCT calculation on the two surfaces employed here is reasonably good. Although the distribution obtained with the H2 PES is affected by the above-discussed problem at the high w_{Cl} range, the maximum of $P(w_{Cl}, \Delta\theta)$ is reproduced remarkably well in all cases. Moreover, it does not present the progressive shift to lower velocities as the result on the PSB2 PES does, which in fact deteriorates the good agreement of the QCT calculation on that surface with the experiment observed at the forward region.

As in the previous QCT investigation of the title reaction at a 0.529 eV collision energy,[11] the triple angle−velocity DCSs have been calculated in the present study for the O(^{1}D) + HCl → OH + Cl reaction channel. The results obtained for the H2 and PSB2 PESs are shown comparatively in Figure 8. The three-dimensional perspective enables the main differences in the dynamical features exhibited in each case to be distinguished. First, the cross section obtained on the PSB2 PES is characterized by a prominent peak in the forward direction at $w_{Cl} \approx$ 1000 m s^{-1} and a considerably less pronounced maximum at somewhat smaller Cl velocities in the backward scattering direction. The corresponding theoretical counterpart on the H2 PES also has a sharp maximum in the forward direction,

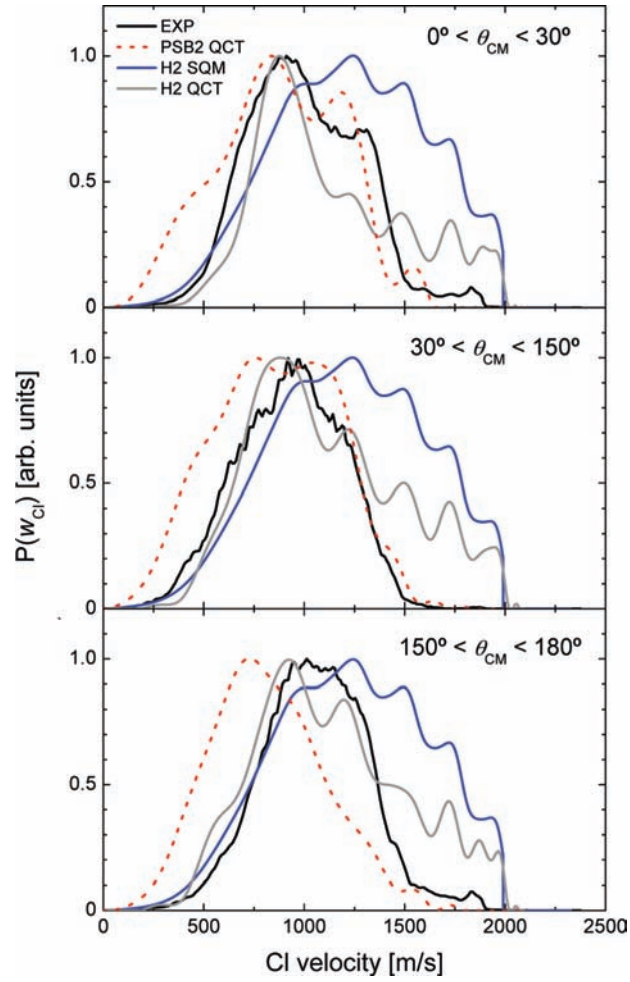

Figure 7. Same as Figure 6 for different scattering angle regions: 0° ≤ θ ≤ 30° (top panel), 30° ≤ θ ≤ 150° (middle panel), and 150° ≤ θ ≤ 180° (bottom panel).

but it is accompanied by secondary structures extended to larger velocities along this scattering direction. In addition, backward scattering is much less pronounced in the H2 PES and is distributed in a wider range of recoil velocities. The most salient difference though is the fact that Cl reaction products with velocities beyond ~1500 m s^{-1} seem to be completely absent in the angle−velocity polar map calculated on the PSB2 PES while on the H2 surface the Cl atom can reach velocities close to the maximum allowed by energy conservation (ca. 2000 m s^{-1}).

The QCT polar maps of Figure 8 can be directly compared with the Abel transformed images shown in Figure 2 of ref 8. In the experimental angle−velocity map, the maximum in the forward direction is centered in and around ~1000 m s^{-1} and then the reactive flux dies out at a Cl recoil velocity of ~1700 m s^{-1}, in fairly good agreement with the results on the PSB2 PES and in contrast with those obtained on the H2 PES.

For comparison purposes, the polar map calculated by the SQM model using eq 7 is represented in Figure 9. As expected, it fails not only in the inherent equiprobability of the scattering in the forward and backward directions, but also in predicting product fragments at velocities near their kinematic limit.

IV. Discussion

The present study has revealed interesting differences in the dynamical observables for the title reaction predicted by

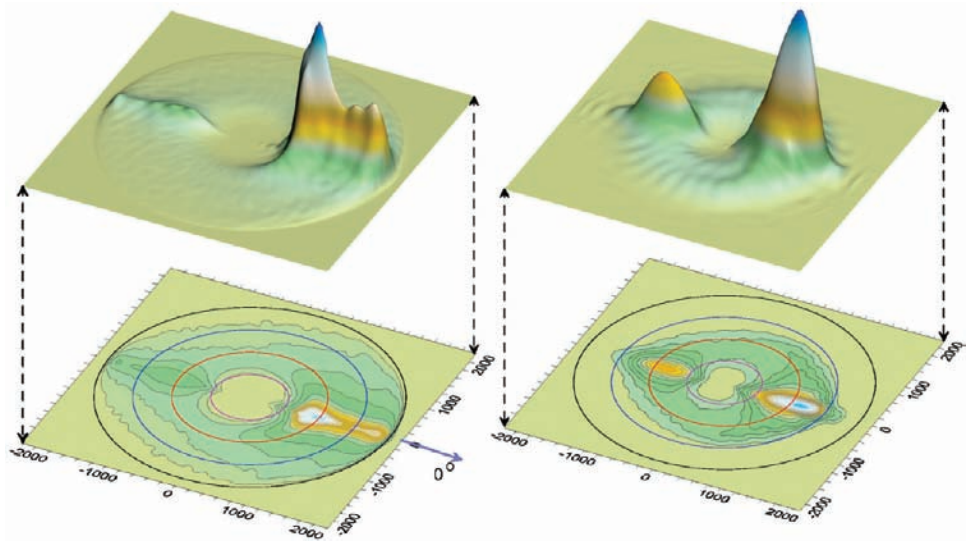

Figure 8. Triple angle−velocity DCSs (both 3D perspective and contour polar plots) for the $O(^1D) + HCl \rightarrow OH + Cl$ reaction at a 0.26 eV collision energy obtained with the QCT approach on the H2 surface (left) and the PSB2 PES (right). The circles on the projection maps represent the contours of the Cl recoil velocities at 500 m s^{-1} (magenta), 1000 m s^{-1} (red), 1500 m s^{-1} (blue), and 2000 m s^{-1} (black).

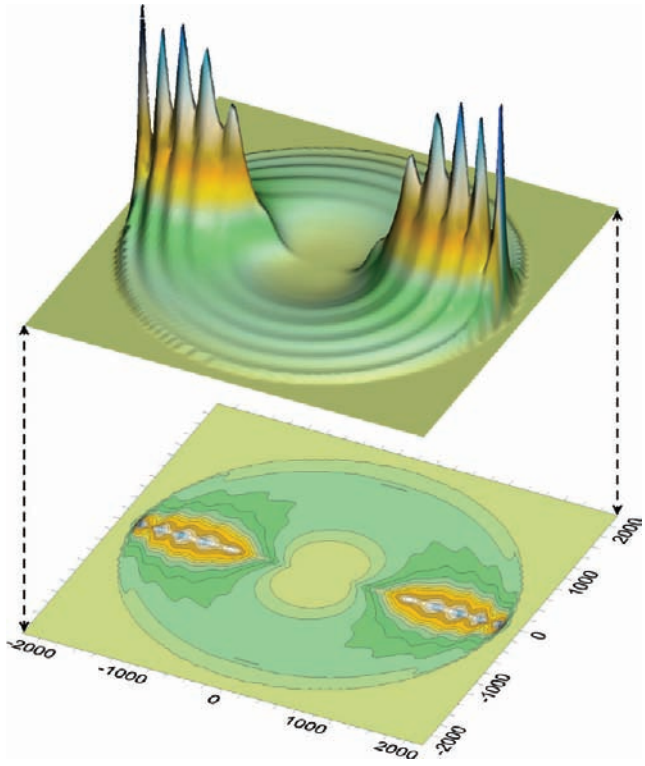

Figure 9. Same as Figure 8 for the SQM result obtained on the H2 surface.

the two PESs employed in the present calculation. Although inverted vibrational cross sections have been obtained at $E_c = 0.26$ eV on both the H2 and PSB2 surfaces, the propensity for the vibrational excitation of the OH fragments formed after the collision is different in each case. In general terms, the calculations on the PSB2 PES render a vibrational distribution biased toward larger values of v'.

However, the most noticeable discrepancy between the dynamical results on both PESs concerns the population of the low rotational states corresponding to the lowest vibrational states $v' = 0$ and 1, which becomes apparent when the rotational distributions are represented. These OH rovibrational states are associated with the fastest recoil velocities of Cl atoms (above 1500 m s^{-1}). The experimental findings of ref 8 by detecting the Cl recoil velocities constitute a most valuable benchmark to asses the quality of both PESs. In this sense, both DCSs and velocity distributions obtained with the PSB2 PES are found to be in better agreement with the corresponding measured quantities.

It is difficult to assess the quality of the two PESs on the basis of the comparison of the present findings with previously measured vibrational and rovibrational distributions. One could argue however (despite the fact that the energy considered here, $E_c = 0.26$ eV, does not correspond to the experimental conditions of refs 2−4) that the scarcely populated low rotational states of the distributions reported for $OH(v' = 0)$ by Luntz[2] possibly resemble the corresponding theoretical distributions obtained with the PSB2 surface (see Figure 2). Analogously, the peak on the $OH(v' = 3)$ state found for the vibrational distributions on that PES (see Figure 1) is consistent with the results reported by Kruus et al.[3]

At this point it is pertinent to compare the topology of both PESs to explain the observed dynamical differences. Reactions involving two heavy atoms and a light one are probably best described by using polar plots in internal Jacobi coordinates of the HH + L product arrangement. In the present case, these plots will represent the cuts of the ClO + H PES for a sequence of different r_{ClO} internuclear distances. This choice is guaranteed by the different time scales of the motion of the light H atom with respect to the relative motion of the much heavier ClO. In these plots the X and Y coordinates are $R_X = R \cos \gamma$ and $R_Y = R \sin \gamma$, where R is the H−ClO distance from the H atom to the CM of the ClO moiety and γ is the Jacobi angle. The left- and right-hand panels of Figure 10 represent snapshots of the potential at various Cl−O distances on the PSB2 and H2 PESs, respectively, and the energy scale is referred to the minimum of the PES at the asymptotic O−HCl separation. On this body-fixed frame, the dynamics of the reaction can be visualized as the approach and retreat of the O atom with respect to the Cl atom along the X axis. In the course of this approach (or retreat), various features of the potential are developed, allowing the H atom to move from the Cl to the O side. More pictorially, the reaction can be described as a successive sequence of landscapes wherein the H atom is roaming around the Cl−O bond.

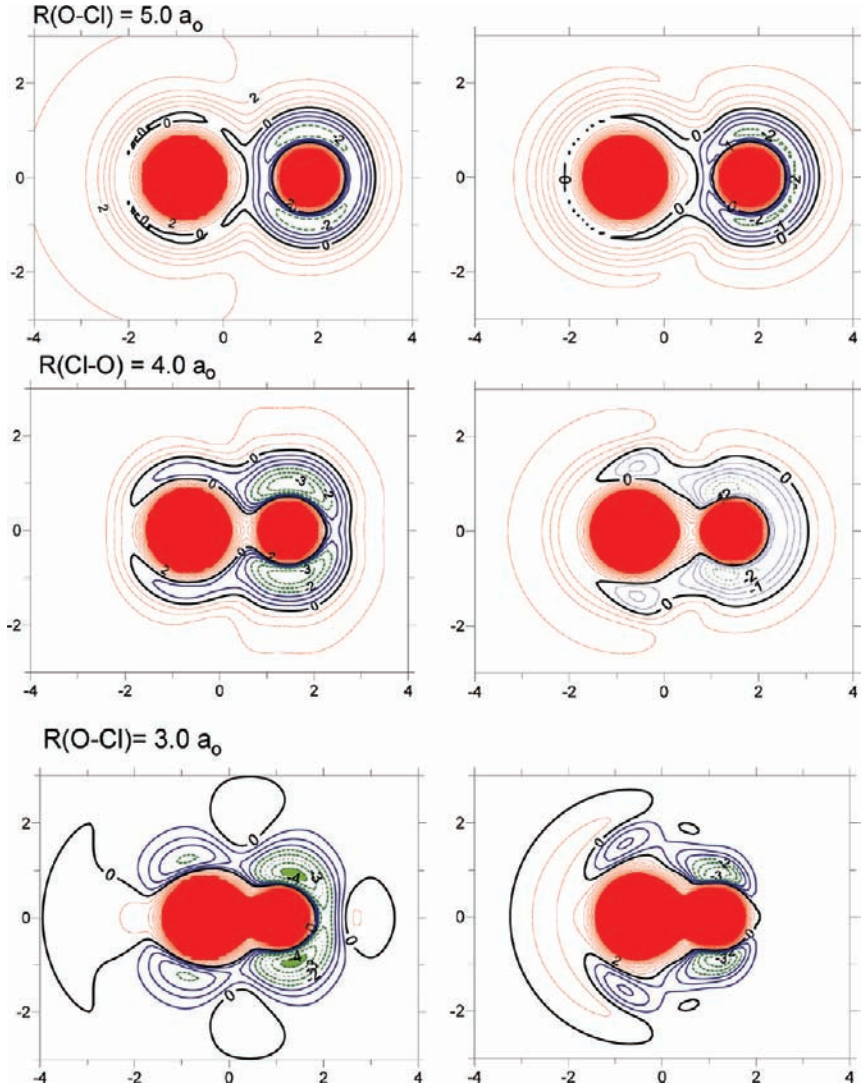

Figure 10. Contour plots of the PSB2 (left panels) and H2 (right panels) PESs for different values of the Cl−O distance (bohr). The energy scale is referred to the minimum of the entrance valley for each PES. Red contours indicate positive energies. Blue contours indicate negative energies but above the OH + Cl asymptotic limit. Dark green (dashed line) contours indicate energies below the minimum of the OH + Cl exit valley. The contours are separated by 0.5 eV.

Initially, at large enough Cl−O distances ($r_{ClO} > 6.0\ a_0$), the H atom can rotate freely around the Cl atom to which it is initially attached, and there exists a barrier preventing the H atom from moving from the Cl to the O atom. As the O atom approaches ($r_{ClO} = 5.0\ a_0$), the motion of the H atom is constrained to move in some regions about the Cl or the O atom. Notice, however, the difference between the two PESs: negative contours on the H2 PES embrace half of the repulsive area around the Cl atom, while on the PSB2 PES this region is much smaller. As a result of this, the hydrogen atom transfer can take place at larger distances on the H2 PES, making possible a direct, stripping-like type of reaction at large impact parameters which does not occur on the PSB2 PES. In fact, this mechanism has not been detected on the latter PES.

As the O approaches the Cl atom at closer distances ($r_{ClO} = 4.0\ a_0$), a double well appears on the H2 PES; the structure corresponds to the HClO and ClOH isomers separated by a transition state. Notice that the H atom is bound to move either between the Cl−O bond or on the opposite side to the Cl atom. On the PSB2 PES the HClO well is not so well developed and actually is an extension of that formed in the ClOH, which is considerably deeper. At even closer distances ($r_{ClO} = 3.0\ a_0$), the differences between the two PESs are apparent: the H atom can move much more freely, and it is more delocalized on the PSB2 PES than on the H2 PES. By inspection of these plots it becomes evident that the chances to transfer the H atom from the Cl to the O side of the complex are larger on the PSB2 PES to form the superexcited ClOH isomer.

In the reverse motion, as the Cl and O atoms retreat from each other, the H atom is likely to remain in the vicinity of the ClOH well. Moreover, this well is deeper and wider on the PSB2 PES than that on the H2 PES (see the frame at $r_{ClO} = 4.0\ a_0$), thus allowing a larger amplitude vibrational motion of the H atom. As the Cl and O part company, this motion will transform into rotation and vibration of the OH molecule solely limited by the conservation of energy. Therefore, higher OH vibrational levels will be comparatively more probable on the PSB2 PES, and those OH products in low v' levels will be formed with a high content of rotational energy. Notice that, in this reverse motion, the HClO well is barely defined on the PSB2 PES, and therefore, its role is less relevant. On the H2 PES, the vibrational motion of the H atom is more constrained and the HClO well is more defined. The net result is the formation of OH with low vibrational ($v' = 0, 1$) and rotational excitation.

As commented on above, most trajectories cannot be described as direct collisions. What effectively happens is that

the Cl−O vibrates a number of times (which can indeed be very large, thus increasing the collision time) before the atoms separate. This motion is, of course, much slower than the stretching and bending of the H atom. While the Cl−O internuclear distance successively stretches and elongates, the various potential landscapes, such as those represented in Figure 10, come into play. The analysis of the results on the PSB2 PES indicates that OH molecules formed in $v' = 0$, 1 visit both wells, while for higher v' the contribution of trajectories confined in the ClOH well becomes increasingly important.

Similar arguments can explain the significant decrease of reactivity on the PSB2 PES for the ClO + H formation. On this PES, the analysis of trajectories shows that the occurrence of this channel takes place exclusively by visiting both wells, much in contrast with the results on the H2 PES where the contribution to the total cross section in this channel from more direct collisions, visiting just one of the wells, was significant. In a way, the collisions leading to ClO + H formation on the PSB2 PES can be considered as the result of long-lived trajectories in which the H manages to escape from the ClOH well, leaving the two heavy atoms bound.

The application of the SQM in this work and the corresponding comparison with both the QCT and experimental results reveal that the $O(^1D)$ + HCl → OH + Cl reaction is far to proceed mainly via the formation of an intermediate long-lived complex. Indications that lead to such conclusions are found in the inversion of the QCT vibrational distributions and the measured distribution of the Cl velocity. There are features which would probably deserve a more detailed discussion. The comparison of both the vibrational and rotational ICSs obtained with the statistical approach and the trajectory calculation on the H2 PES reveals some aspects in common. In spite of the fact that the lowest vibrational states $v' = 0$ and 1 present a total population and an energy distribution among the corresponding rotational states which are clearly far to be described by statistical means, the dynamics of higher vibrational states such as $v' = 4$ and $v' = 5$ seems to be more amenable to a statistical treatment. The SQM−QCT comparison for the vibrational distributions calculated on the H2 surface shown in Figure 1 resembles the situation found for the Si + O_2 collision.[46] For this reaction, the dynamics was found to shift from a direct pathway to an intermediate-complex-mediated mechanism as either the initial rotational excitation of the O_2 reactant or the collision energy increases. Vibrational distributions calculated with a trajectory approach also exhibit a slight inversion in the population of SiO(v') states, in clear discrepancy with the statistical predictions for the low vibrational states, but the agreement seems to improve as v' increases.

The ratio between the forward and backward peaks observed in the experimental DCS is sufficiently low to compare better with the statistical result than the corresponding QCT distribution, affected by a too large tendency for the forward direction. A reasonable question might be whether this can change when the energy varies. Experimental DCSs have been found to become symmetric as the collision energy decreases from 0.2775 to 0.1821 eV.[9] The comparison established here at 0.260 eV corresponds therefore to the case with the largest degree of asymmetry around $\theta \approx 90°$ in the measured angular cross section. Despite that, the agreement found between the SQM result and the experimental DCS is not bad. On the other hand, the CM translational energy release distributions and the contour plots reported in ref 9 seem not to suggest that a complex-forming mechanism might acquire a major relevance as the energy changes.

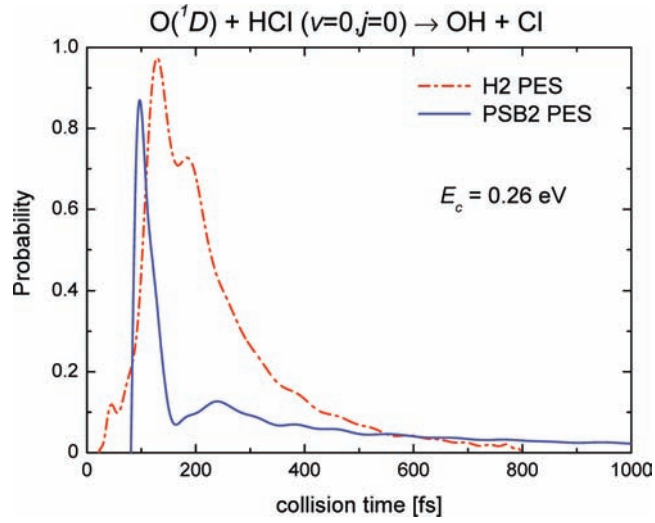

Figure 11. Comparison between the collision time distributions on the H2 (dashed−dotted line) and PSB2 (solid line) PESs for the $O(^1D)$ + HCl → OH + Cl reaction at a 0.26 eV collision energy.

One more interesting point is why the statistical calculations deviate from the dynamical behavior evinced by the QCT calculations in the case of the PSB2 PES. A likely requirement for a statistical description is that the collision time, i.e., the time that the three atoms stay together, should be long enough for a complete randomization of the vector and scalar properties. In the present work, we have calculated the QCT distributions of collision times on the two PESs that are comparatively represented in Figure 11. The procedure to determine the collision time is the same as that employed in ref 24. As can be seen, the differences between the two curves are indeed considerable. The results on the H2 PES are very close to those obtained before.[24] The curve has a sharp maximum at ∼120 fs, and after a shoulder, it decreases monotonically at larger times. However, one can hardly find trajectories with more than 800 fs, and overall, the average lifetime is ∼260 fs.

In strong contrast, the curve on the PSB2 PES is clearly bimodal: a very sharp and narrow peak at ∼100 fs and a secondary maximum at 250 fs followed by a long tail that extends up to 5 ps. The average lifetime is ∼700 fs, with 86% of the trajectories with a collision time $\tau_{coll} \leq 1.5$ ps. It is immediate that those collisions pertaining to the first peak do not live long enough for the energy to be randomized and can be described as essentially direct trajectories in which the Cl and O approach and retreat within one or two vibrational periods. The analysis of these trajectories shows that they only visit the ClOH well. Those pertaining to the long tail visit both wells, and the reaction takes place after several vibrations of the OCl bond while the H atom is roaming around the heavy atoms. As such, they are expected to follow a statistical pattern. By inspection of the collision times on the H2 PES, it becomes apparent why the overall dynamical behavior is better described, at least in some aspects, by statistical approaches. In none of the PESs, however, can the reaction be expected to comply with the assumption of proceeding exclusively via the formation of truly long-lived complexes, and therefore, it is hardly surprising that the SQM or SQCT models do not reproduce the QCT dynamical findings.

Finally, as for the ClO + H product channel, the QCT results on the H2 PES[11] at 529 meV could reproduce very well not only the ClO LAB angular distributions, but also the more stringent TOF spectra at various LAB angles measured by Balucani et al.[7] The QCT calculations on the PSB2 PES predict

a much smaller branching ratio for ClO formation as compared to that found on the H2 PES (0.09 vs 0.29), at variance with the experimental determinations of Matusmi et al.[5] Apart from this overall factor, the shapes of the vibrational and rovibrational distributions are similar. In neither case is there a vibrational inversion, and the rotational distributions for each vibrational state are not very different in shape from those described by the statistical model. Moreover, the QCT distributions on the H2 PES are almost in quantitative agreement with those obtained with the SQM approach. The SQCT rovibrational distribution on the PSB2 PES, which is similar to that on the H2 PES, disagrees with the QCT distributions in their absolute value, but the habits are also similar. This shape is typical of insertion processes, in which the final energy redistribution among the product states can be explained on statistical grounds. The comparatively larger number of $ClO(v'', j'')$ rovibrational states could possibly favor a statistical description of the dynamics for this channel. The forward−backward symmetry of both QCT[11] and experimental[7] DCSs observed at 0.53 eV for the $O(^1D) + HCl \rightarrow ClO + H$ reaction could also be a further indication of a complex-forming mechanism. The analysis of collision times seems to support this assumption. Interestingly, the average lifetime on the PSB2 PES for ClO formation is ∼820 fs, even larger than for the OH + Cl product channel, signifying that most of the ClO products are formed via a long-lived complex. On the H2 PES the average lifetime is much shorter, ∼220 fs with 95% of the trajectories with $\tau_{coll} \leq 500$ fs. Given the extreme difficulty in carrying out EQM calculations for this reaction channel, the application of statistical techniques, such as the SQM or SQCT[35−37] approaches, would constitute a very useful alternative. Work in this direction is currently in progress.

V. Conclusions

In this work we have analyzed the dynamics of the $O(^1D) + HCl$ reaction at a 0.26 eV collision energy by means of the quasiclassical trajectory method and two statistical (quantum and quasiclassical) approaches employing two different potential energy surfaces: that by Hernández, Laganà, and co-workers, here denoted H2, and the PSB2 by Peterson, Bowman, and co-workers. The theoretical results have been compared with recent measurements in which the angle−velocity DCSs have been determined for the OH + Cl product channel by detecting the $Cl(^2P_{3/2})$ atoms using an ion imaging technique.

Trajectory results on both surfaces have been found to differ significantly for the $O(^1D) + HCl \rightarrow OH + Cl$ reaction. Specifically, the results on the PSB2 surface seem to reproduce better the observed angle−velocity distributions of the Cl atoms. In turn, the quasiclassical results on the H2 PES for this reaction channel predict a larger amount of chlorine atoms at high velocities and a too pronounced scattering along the forward direction than that found experimentally. The calculations on the H2 PES predict a OH state distribution wherein the population of low rotational levels in the $v' = 0, 1$ manifolds is significant. In contrast, on the PSB2 PES these states have a negligible cross section. The experimental velocity distributions and polar maps seem to support the latter results clearly.

The energy disposal mechanisms occurring during the reaction which leads to the formation of OH cannot be well described by statistical considerations. The measured distribution of the product Cl fragment velocity, for instance, does not agree with the statistical description. According to the SQM approach, the Cl atoms should be formed in the reaction with a faster velocity than the experimental study concludes. The statistical results on the PSB2 are overall rather similar to those obtained on the H2 PES, something that is not surprising given the fact that the main discrepancies between both PESs are in the region of the HOCl and HClO wells, which are not contemplated in the statistical treatment.

The analysis of classical collision times on both PESs indicates that the PSB2 PES has a bimodal character, with an important contribution from direct, short-lived mechanisms, whereas that obtained on the H2 PES has a single maximum with a somewhat shorter tail.

The production of ClO fragments displays, however, significant features of a complex-forming reaction mechanism.

Acknowledgment. We dedicate this work to Professor Vicenzo Aquilanti, whose long scientific career has served of inspiration and encouragement for many scientists in the field of reaction dynamics. We thank Prof. T. Suzuki, Prof. G. G. Balint-Kurti, and Dr. M. Hankel for sending us their results and useful discussions. This work has been funded by the MEC (Spain) under Projects CTQ2005-09185-C02-02, CTQ2008-02578, and FIS2007-62006. P.B. and P.G.J. also acknowledge support from Fellowship Grants BES-2006-11976 and AP2006-03740, respectively.

References and Notes

(1) Sorokin, V. I.; Gritsan, N. P.; Chichinin, A. I. *J. Chem. Phys.* **1998**, *108*, 8995–9003.
(2) Luntz, A. C. *J. Chem. Phys.* **1980**, *73*, 5393.
(3) Kruus, E. J.; Niefer, B. I.; Sloan, J. J. *J. Chem. Phys.* **1988**, *88*, 985.
(4) Park, C. R.; Wiesenfeld, J. R. *Chem. Phys. Lett.* **1989**, *163*, 230.
(5) Matsumi, Y.; Tonokura, K.; Kawasaki, M.; Tsuji, K.; Obi, K. *J. Chem. Phys.* **1993**, *98*, 8330.
(6) Alexander, A. J.; Brouard, M.; Rayner, S. P.; Simons, J. P. *Chem. Phys.* **1996**, *207*, 215.
(7) Balucani, N.; Beneventi, L.; Casavecchia, P.; Volpi, G. G. *Chem. Phys. Lett.* **1991**, *180*, 34.
(8) Kohguchi, H.; Suzuki, T. *ChemPhysChem* **2006**, *7*, 1250.
(9) Kohguchi, H.; Suzuki, T.; Nanbu, S.; Ishida, T.; Mil'nikov, G. V.; Oloyede, P.; Nakamura, H. *J. Phys. Chem. A* **2008**, *112*, 818.
(10) Hernández, M. L.; Redondo, C.; Laganà, A.; Ochoa de Aspuru, G.; Rosi, M.; Sgamellotti, A. *J. Chem. Phys.* **1996**, *105*, 2710.
(11) Martínez, T.; Hernández, M. L.; Alvariño, J. M.; Laganà, A.; Aoiz, F. J.; Menéndez, M.; Verdasco, E. *Phys. Chem. Chem. Phys.* **2000**, *2*, 589.
(12) Skokov, S.; Peterson, K. A.; Bowman, J. M. *J. Chem. Phys.* **1998**, *109*, 2662.
(13) Peterson, K. A.; Skokov, S.; Bowman, J. M. *J. Chem. Phys.* **1999**, *111*, 7446.
(14) Skokov, S.; Peterson, K. A.; Bowman, J. M. *Chem. Phys. Lett.* **1999**, *312*, 494.
(15) Bittererova, M.; Bowman, J.; Peterson, K. *J. Chem. Phys.* **2000**, *113*, 6186.
(16) Christoffel, K. M.; Bowman, J. M. *J. Chem. Phys.* **2002**, *116*, 4842.
(17) Nanbu, S.; Aoyagi, M.; Kamisaka, H.; Nakamura, H.; Bian, W.; Tanaka, K. *J. Theor. Comput. Chem.* **2002**, *1*, 263.
(18) Lin, S. Y.; Han, K.-L.; Zhang, J. Z. H. *Phys. Chem. Chem. Phys.* **2000**, *2*, 2529.
(19) Schinke, R. *J. Chem. Phys.* **1984**, *80*, 5510.
(20) Laganà, A.; Ochoa de Aspuru, G.; García, E. *J. Phys. Chem.* **1995**, *99*, 17139.
(21) Alvariño, J. M.; Bolloni, A.; Hernández, M. L.; Laganà, A. *J. Phys. Chem. A* **1998**, *102*, 10199.
(22) Christoffel, K. M.; Kim, Y.; Skokov, S.; Bowman, J. M.; Gray, S. K. *Chem. Phys. Lett.* **1999**, *315*, 275.
(23) Alvariño, J. M.; Rodríguez, A.; Laganà, A.; Hernández, M. L. *Chem. Phys. Lett.* **1999**, *313*, 299.
(24) Martinez, T.; Hernández, M. L.; Alvariño, J. M.; Aoiz, F. J.; Sáez Rábanos, V. *J. Chem. Phys.* **2003**, *119*, 7871.
(25) Lin, S. Y.; Han, K.-L.; Zhang, J. Z. H. *Chem. Phys. Lett.* **2000**, *324*, 122.
(26) Bittererova, M.; Bowman, J. *J. Chem. Phys.* **2000**, *113*, 1.
(27) Kamisaka, H.; Nakamura, H.; Nanbu, S.; Aoyagi, M.; Bian, W.; Tanaka, K. *J. Theor. Comput. Chem.* **2002**, *1*, 275.
(28) Kamisaka, H.; Nakamura, H.; Nanbu, S.; Aoyagi, M.; Bian, W.; Tanaka, K. *J. Theor. Comput. Chem.* **2002**, *1*, 285.

(29) Yang, H.; Han, K.-L.; Nanbu, S.; Nakamura, H.; Balint-Kurti, G. G.; Zhang, H.; Smith, S. C.; Hankel, M. *J. Phys. Chem. A* **2008**, *112*, 7947.
(30) Piermarini, V.; Balint-Kurti, G. G.; Gray, S. K.; Gogtas, F.; Laganà, A.; Hernández, M. L. *J. Phys. Chem. A* **2001**, *105*, 5743.
(31) Piermarini, V.; Laganà, A.; Balint-Kurti, G. G. *Phys. Chem. Chem. Phys.* **2001**, *3*, 4515.
(32) Lin, S. Y.; Park, S. C. *Bull. Korean Chem. Soc.* **2002**, *23*, 229.
(33) Rackham, E. J.; Huarte-Larrañaga, F.; Manolopoulos, D. E. *Chem. Phys. Lett.* **2001**, *343*, 356.
(34) Rackham, E. J.; González-Lezana, T.; Manolopoulos, D. E. *J. Chem. Phys.* **2003**, *119*, 12895.
(35) Aoiz, F. J.; Rábanos, V. S.; González-Lezana, T.; Manolopoulos, D. E. *J. Chem. Phys.* **2007**, *126*, 161101.
(36) Aoiz, F. J.; González-Lezana, T.; Rábanos, V. S. *J. Chem. Phys.* **2007**, *127*, 174109.
(37) Aoiz, F. J.; González-Lezana, T.; Rábanos, V. S. *J. Chem. Phys.* **2008**, *129*, 094305.
(38) Bañares, L.; F. J.; Aoiz, P. H.; Bussery-Honvault, B.; Launay, J.-M. *J. Chem. Phys.* **2003**, *118*, 565.
(39) Bonnet, L.; Rayez, J.-C. *Chem. Phys. Lett.* **1997**, *277*, 183.
(40) Bonnet, L.; Rayez, J.-C. *Chem. Phys. Lett.* **2004**, *397*, 106.
(41) Aoiz, F. J.; Herrero, V. J.; Rábanos, V. S. *J. Chem. Phys.* **1992**, *97*, 7423.
(42) Aoiz, F. J.; Verdasco, E.; Rábanos, V. S.; Loesch, H.; Menéndez, M.; Stienkemeier, F. *Phys. Chem. Chem. Phys.* **2000**, *4*, 541.
(43) González-Lezana, T. *Int. Rev. Phys. Chem.* **2007**, *26*, 29.
(44) Bañares, L.; Aoiz, F. J.; González-Lezana, T.; Herrero, V. J.; Tanarro, I. *J. Chem. Phys.* **2005**, *123*, 224301.
(45) Bargueño, P.; González-Lezana, T.; Larrégaray, P.; Bonnet, L.; Rayez, J.-C.; Hankel, M.; Smith, S. C.; Meijer, A. J. H. M. *J. Chem. Phys.* **2008**, *128*, 244308.
(46) Dayou, F.; Larrégaray, P.; Bonnet, L.; Rayez, J.-C.; Arenas, P. N.; González-Lezana, T. *J. Chem. Phys.* **2008**, *128*, 174307.

JP902336S